Materials Horizons

ROYAL SOCIETY OF CHEMISTRY

COMMUNICATION

View Article Online
View Journal

Cite this: DOI: 10.1039/d5mh02318a

Received 4th December 2025,
Accepted 17th December 2025

DOI: 10.1039/d5mh02318a

rsc.li/materials-horizons

Post-functionalization modification as a modular strategy for size-selective fluorescence response of single-walled carbon nanotubes to polycyclic aromatic hydrocarbons

Srestha Basu,[abc] Dominik Just,[d] Adi Hendler-Neumark,[a] Dawid Janas [d] and Gili Bisker *[aefgh]

Single-walled carbon nanotubes (SWCNTs) with tailored functionalization serve as optically responsive nanoparticles, but when encapsulated by chirality-selective polymers, they often remain inert to analytes. To expand their utility, we developed a post-functionalization modification (PFM) strategy introducing oxygen defects into chirality-pure (6,5) and (7,5) SWCNTs suspended by PFO-BPy6,6′ and PFO-FH, respectively. UV exposure in the presence of sodium hypochlorite (NaClO) partially displaces the polymer corona, confirmed by low-temperature fluorescence, Raman spectroscopy, dynamic light scattering, and transmission electron microscopy. To probe corona displacement, riboflavin (RB) was employed as a fluorescent reporter for the exposed SWCNT surface. Minimal RB quenching was observed with (6,5) and (7,5) SWCNTs treated with low NaClO concentration (0.01%), indicating high coverage, while dispersions treated with higher NaClO concentration (0.055%) showed strong RB quenching, reflecting reduced coverage. This trend establishes NaClO concentration as a handle to tune corona coverage. We further show that surface coverage modulates size-selective adsorption of polyaromatic hydrocarbons (PAHs). At intermediate NaClO treatment (0.02%), PFM-SWCNTs responded selectively to naphthalene (2-ring PAH), while higher treatment (0.055%) enabled response to naphthalene, fluorene, and pyrene (2, 3, and 4-ring PAH). These findings demonstrate that PFM enables controllable surface coverage and size-selective PAH interactions, broadening SWCNTs utility as optical nanoprobes.

New concepts

While chirality-pure single-walled carbon nanotubes (SWCNTs) have significantly advanced the understanding of structure–property relationships and enabled precise optical studies, their strong polymer encapsulation – essential for achieving high-purity separation – can nevertheless reduce interfacial reactivity, limiting their adaptability in molecular recognition. To address this challenge, we introduce a new concept termed post-functionalization modification (PFM) strategy that finely controls the reactivity of polymer-encapsulated monochiral SWCNTs without perturbing their chirality. PFM employs sodium hypochlorite (NaClO) under UV irradiation to simultaneously induce partial corona displacement and oxygen-defect incorporation, thereby generating a tunable interface that preserves the nanotubes' optical and chirality integrity while enhancing accessibility to external analytes. By explicitly varying the NaClO concentration, the degree of corona disruption is controllably tuned: higher NaClO concentrations produce more extensive corona displacement (*i.e.*, lower polymer surface coverage) and therefore enhance accessibility to larger-sized analytes, whereas intermediate NaClO levels leave more of the corona intact and favor interactions with relatively smaller molecules. This NaClO-dependent tunability enables size-selective fluorescence responses toward polycyclic aromatic hydrocarbons (PAHs), demonstrating controlled molecular recognition in systems that were previously functionally limited. Collectively, PFM provides a modular, generalizable route to impart tunable chemical reactivity to monochiral SWCNTs thereby substantially expanding their utility in organic environments.

1. Introduction

Polydispersity among nanoscale particles influences their functional performance, presenting both challenges and opportunities for applications.[1] In single-walled carbon nanotubes

[a] School of Biomedical Engineering, Faculty of Engineering, Tel Aviv University, Tel Aviv 6997801, Israel. E-mail: bisker@tauex.tau.ac.il
[b] Biophysical Sciences Group, Saha Institute of Nuclear Physics, 1/AF Bidhannagar, Kolkata 700064, India
[c] Chemical Sciences Division, Homi Bhabha National Institute, Mumbai 400094, India
[d] Department of Chemistry, Silesian University of Technology, B. Krzywoustego 4, 44-100 Gliwice, Poland
[e] Center for Physics and Chemistry of Living Systems, Tel Aviv University, Tel Aviv 6997801, Israel
[f] Center for Nanoscience and Nanotechnology, Tel Aviv University, Tel Aviv 6997801, Israel
[g] Center for Light–Matter Interaction, Tel Aviv University, Tel Aviv 6997801, Israel
[h] Sagol School of Neuroscience, Tel Aviv University, Tel Aviv 6997801, Israel

(SWCNTs), the coexistence of multiple chiralities, each associated with a different diameter, gives rise to dispersions with diverse optical and electronic properties.[2–7] While such inherent heterogeneity has been leveraged in various applications,[8–13] it can also complicate the establishment of precise structure–property relationships, as ensemble-averaged properties may often obscure the behavior of individual species. Thus, to achieve greater control and predictability in specific applications, efforts have been directed toward isolating monochiral SWCNT populations, enabling more uniform properties and refined functionality.[14–22]

To achieve this, several techniques have been employed, including aqueous two-phase extraction of chirality-pure SWCNTs,[23–26] gel chromatography-based selective adsorption of chirality-pure SWCNTs in the gel medium,[27] and adsorption strategies that leverage chiral angle and diameter selectivity.[28] In this context, another widely adopted approach involves chirality-selective extraction, wherein conjugated polymers with tailored chemical affinity isolate SWCNTs of a specific chirality, enabling precise separation and enhanced application outcomes.[16,29–31] This technique is particularly prominent in organic media, where the non-polar nature of the commonly used polymers aids in selective extraction. For instance, poly(9,9′-dioctylfluorenyl-2,7-diyl-*alt*-6,6′-(2,2′-bipyridine)) (PFO-BPy6,6′) has been effectively employed to selectively extract (6,5) SWCNTs, while poly(9,9′-dioctylfluorenyl-2,7-diyl) (PFO) has been utilized for the selective extraction of (7,5) SWCNTs.[16] However, the strong affinity and tight encapsulation of these polymers around specific chiralities[32] could result in steric hindrances, reducing the SWCNT accessibility to exogenously introduced analytes, thereby limiting their reactivity in organic environments.

Therefore, to extend the applicability of monochiral SWCNTs in organic environments, it is essential to enhance their responsiveness to chemical species. A promising approach to achieve this, whether for molecular or nanoscale targets, is post-synthetic/functionalization modification (PFM), which enables improved interactions with target analytes. PFM has been widely employed across various nanoscale systems, including atomic clusters,[33,34] quantum dots,[35,36] carbon dots,[37] and metal–organic frameworks (MOFs),[38,39] to imbue them with additional functionalities. For instance, in histidine-stabilized gold atomic clusters, ligand exchange reactions have been used to replace histidine with cysteine, modulating their emission wavelength.[33] Similarly, surface complexation reactions have been utilized in quantum dots to fine-tune fluorescence,[40,41] while doping carbon dots with specific atoms has enabled multi-tunable emission.[42] In the case of MOFs, strategic incorporation of reactive molecules has been employed to enhance their chemical reactivity.[43]

To this end, an effective strategy for imparting reactivity to SWCNTs involves introducing defects through PFM. Recent studies have demonstrated that incorporating functional groups into SWCNTs enhances their specific reactivity toward external analytes.[44–57] Our laboratory has recently validated the application of PFM to SWCNTs, demonstrating that SWCNTs dispersed in aqueous phases with surfactants can be rendered responsive to exogenously added target molecules through the incorporation of oxygen defects.[58,59] Notably, pristine SWCNTs lacking such defects exhibited no response under similar conditions, underscoring the transformative role of defect engineering in enabling such interactions. These findings not only substantiate the feasibility of PFM in SWCNTs but also open avenues for imparting new functionalities and responsiveness, thereby broadening their application potential. However, two key gaps remain: most demonstrations have been limited to aqueous dispersions rather than organic media, and the tunability of functionalization levels for controlled analyte interactions has yet to be fully explored.

Building on this, expanding the interactive potential of monochiral SWCNTs in organic media through PFM addresses two critical challenges: it circumvents the issue of polydispersity by utilizing monochiral SWCNTs, and it overcomes the limitations imposed by the tight binding of polymers, which otherwise render SWCNTs unresponsive to external analytes. The ability of SWCNTs to interact effectively in organic media, a largely unexplored area in the literature, could pave the way for novel applications. Further, if corona displacement in SWCNTs could be systematically tuned, it would open a powerful route to control their interactions with external analytes. Such tunability could allow recognition of smaller molecules under conditions of higher surface coverage, while reduced coverage could broaden the spectrum of accessible analytes, including larger aromatic systems. This level of control would not only expand the functional versatility of monochiral SWCNTs in organic media but also establish a design principle for tailoring sensing behavior toward either highly specific or more universal detection modes. Achieving such adaptive responsiveness would position PFM-treated SWCNTs as promising platforms for advanced molecular sensing and next-generation optical nanoprobes in complex environments.

Here, we demonstrate the application of PFM to SWCNTs (dispersed in organic media) using sodium hypochlorite (NaClO) and UV exposure to introduce oxygen defects in monochiral SWCNTs. Chirality-pure (6,5) and (7,5) SWCNTs were utilized and dispersed with the PFO derivatives PFO-BPy6,6′ and PFO-FH, respectively. The treatment with NaClO and UV exposure triggered two processes: (i) partial displacement of the polymer corona and (ii) incorporation of oxygen defects into the SWCNTs. Raman spectroscopy, in conjunction with dynamic light scattering (DLS) studies, transmission electron microscopy (TEM), and low-temperature fluorescence spectroscopy, confirmed the successful displacement of the polymer corona and the introduction of oxygen defects. To evaluate the extent of corona displacement, riboflavin (RB) was employed as a fluorescence reporter, where minimal quenching at low NaClO concentration indicated dense coverage, while strong quenching at higher concentrations revealed reduced coverage. This tunability was consistent across both chiralities, establishing NaClO as a handle for modulating corona density. To assess how this impacts analyte interactions, we exposed PFM-SWCNTs to a series of polyaromatic hydrocarbons (PAHs), including naphthalene (Naph), phenanthrene (Phen), pyrene, and fluorene. While unmodified SWCNTs showed minimal response, PFM-SWCNTs exhibited a strong fluorescence

decrease. Importantly, intermediate corona coverage enabled selective response to smaller PAHs such as naphthalene, whereas reduced coverage allowed broader response, including fluorene and pyrene. Control studies with monoaromatic and aliphatic molecules produced no significant effect, while comparing styrene (monoaromatic) and polystyrene (polyaromatic) reinforced the necessity of multiple aromatic rings for eliciting fluorescence modulation. These findings highlight the pivotal role of PFM in enabling and tuning interactions between SWCNTs and exogenous molecules through corona modification and defect incorporation. This approach not only imparts reactivity to otherwise inert SWCNTs but also introduces a strategy for controllable, size-selective detection of aromatic analytes, thereby expanding the functional versatility of SWCNTs in organic media.

2. Experimental section

2.1. Separation of (6,5) and (7,5) SWCNTs

1.5 mg of the SG65i CoMoCAT SWCNTs and 6 mg of PFO-BPy6,6′ or 9 mg of PFO-FH were combined with 5 mL of toluene in a glass vial. The mixture was homogenized in a mild bath sonicator for 15 minutes (Polsonic, Sonic-2, 250 W) at 5 °C and then more vigorous tip sonication (Hielscher UP200St ultrasonic generator) was used for 8 minutes at a power of 30 W for selective solubilization of SWCNTs. As-obtained suspension of SWCNTs was centrifuged at 10 000 rpm (15 314 × g) for 2 minutes to precipitate the undesired SWCNTs and polymer aggregates. 80% of the generated supernatant containing purified SWCNTs was collected and used in further experiments.

2.2. Optical absorption

Absorption spectra were recorded using a Shimadzu UV-3600 Plus UV-vis-NIR spectrophotometer over a wavelength range of 300 to 1400 nm.

2.3. Post-functionalization modification (PFM) of SWCNTs

PFM of SWCNTs was pursued by diluting (6,5) and (7,5) SWCNTs in toluene to a concentration of 28.5 μg L^{-1}. To these samples, 10 μL of 11% NaClO was added, followed by UV irradiation at 365 nm for 10 min in the presence of tetraethylammonium bromide (∼1 mg) as a phase-transfer catalyst. This treatment led to a decrease in the E_{11} fluorescence of (6,5) and (7,5) SWCNTs when excited at 560 nm and 650 nm, respectively, as well as the emergence of the E_{11}^{*} fluorescence peak (measured at 77 K) and the typical Raman peaks associated with defects incorporation.

2.4. Fluorescence

Fluorescence measurements were performed using a 96-well plate positioned on the stage of an inverted Olympus IX73 microscope. Excitation was provided by a supercontinuum laser (NKT Photonics, Super-K Extreme) at 560 and 650 nm. Emission spectra were analyzed using a Spectra Pro HRS-300 spectrograph (Princeton Instruments) equipped with a 150 g mm^{-1} grating and a 500 μm slit width. The fluorescence intensity spectra were recorded using a 1D InGaAs array detector (PylonIR, Teledyne Princeton Instruments) with an exposure time of 3 s. Excitation–emission maps were generated by scanning excitation wavelengths from 450 nm to 800 nm in 2 nm increments using a supercontinuum white-light laser (NKT Photonics, Super-K Extreme). All spectra were background-subtracted against blank toluene. Additional fluorescence measurements were conducted with an FLS1000 photoluminescence spectrometer (Edinburgh Instruments), featuring an ozone-free Xe lamp, kinematic triple-grating turret monochromators, and NIR-PMT detectors capable of photon counting up to ∼1700 nm. For fluorescence measurements at low temperature, a software-controlled cryostat was used to maintain the temperature at 77 K, and the samples were placed in electron paramagnetic resonance (EPR) tubes for the measurement.

To assess the fluorescence response of (6,5) and (7,5) SWCNTs to PAHs, samples of 200 μL of toluene containing 28.5 μg L^{-1} SWCNTs were combined with PAHs at concentrations ranging from 80 to 400 μM, and the resulting emission spectra were recorded.

2.5. Transmission electron microscopy

TEM analysis was performed using a JEOL 2100F microscope with an accelerating voltage of 200 kV. Image processing was carried out using Gatan Digital Micrograph software. For sample preparation, 7 μL of 100 μg L^{-1} (6,5) and (7,5) SWCNTs were drop-cast onto a carbon-coated copper grid.

2.6. Raman spectroscopy

Raman spectra were recorded using a LabRam HR Evolution spectrometer. The (6,5) SWCNT and (7,5) SWCNT samples were drop-cast onto glass slides and illuminated with a 532 nm laser and a 633 nm laser, respectively. Data acquisition was performed using a ×100 objective lens with a laser power set to 100 mW.

2.7. Dynamic light scattering

Dynamic light scattering (DLS) measurements were performed using a Malvern Zetasizer Nano ZS90 (Model No. ZEN3690) equipped with a red He–Ne gas laser (λ = 633 nm) at a controlled temperature of 25 °C. The concentrations of (6,5) and (7,5) SWCNTs were maintained at 28.5 mg L^{-1}. An anisotropic rigid-rod model, as established in previous studies, was used to determine the effective hydrodynamic diameter of the SWCNTs.[60–62]

2.8. Statistical analysis

All fluorescence experiments were performed in triplicate, and the displayed spectra represent the average of three independently acquired measurements. Spectral data were analyzed and plotted using Origin software, while excitation and emission profiles were generated using MATLAB.

3. Results and discussions

Near-monochiral (6,5) and (7,5) SWCNTs were obtained by Conjugated Polymer Extraction (CPE) using self-synthesized poly(9,9-dioctylfluorene-2,7-diyl-*alt*-6,6′-{2,2′-bipyridine}) (PFO-BPy6,6′) and poly(2,7-(9,9′-dioctylfluorene)-*alt*-2,7-(-9,9′-hexylfluorene)) (PFO-FH), respectively (Fig. S1). The UV-vis-NIR absorption spectra of PFO-BPy6,6′ (6,5) SWCNTs and PFO-FH (7,5) SWCNTs exhibited distinct absorption peaks at 1002 nm and 1044 nm, respectively, corresponding to the E_{11} transitions of the (6,5)[63] and (7,5)[64] SWCNTs (Fig. S2A and B). Similarly, the fluorescence spectra of PFO-BPy6,6′ (6,5) SWCNTs and PFO-FH (7,5) SWCNTs exhibited emissions at 1002 nm and 1046 nm when excited at 560 nm[63] and 650 nm,[64] respectively (Fig. S3A and B). The excitation and emission maps of these samples showed distinct peaks corresponding to the E_{11} transitions of the (6,5) and (7,5) SWCNTs (Fig. S3C and D). The absence of additional excitation–emission peaks under other excitation wavelengths confirmed the lack of other chiralities, validating the successful separation of (6,5) and (7,5) SWCNTs.

Further, atomic force microscopy (AFM) was conducted to gain morphological insights into PFO-BPy6,6′ (6,5) SWCNTs and PFO-FH (7,5) SWCNTs. AFM images of PFO-BPy6,6′ (6,5) SWCNTs revealed nanotubes with heights of 0.8 ± 0.2 nm. Similarly, AFM images of PFO-FH (7,5) SWCNTs showed nanotubes with heights of 0.9 ± 0.3 nm (Fig. S4A and B).

To introduce additional functionalities to SWCNTs, a small volume of concentrated NaClO was added to the PFO-BPy6,6′ (6,5) and PFO-FH (7,5) SWCNTs dispersed in toluene, followed by exposure to UV irradiation at 365 nm. The process aimed to generate singlet oxygen in the aqueous phase, which, owing to its higher solubility in organic solvents compared to aqueous ones,[65] could diffuse in the toluene medium containing the SWCNTs. Once in the organic phase, the singlet oxygen was expected to react with the SWCNTs, facilitating the incorporation of oxygen defects, as reported in previous studies. These oxygen defects typically manifest as ether-bridged oxygen atoms or as epoxide adducts within the SWCNT structure.[51] Further, in our experiments, singlet oxygen was transferred from the aqueous NaClO phase into the toluene-dispersed SWCNTs through the combined effects of UV irradiation and a phase-transfer catalyst, and the PFO-based polymer wrappings were considered stable in toluene,[66] with no polymer unwrapping expected under these conditions.

Following treatment with NaClO and UV irradiation, the UV-vis-NIR absorption spectra of (6,5) and (7,5) SWCNTs were recorded. The peaks at 998 nm and 1042 nm, corresponding to the E_{11} transitions of (6,5) and (7,5) SWCNTs, respectively, exhibited a decrease in absorption (Fig. S5). This could be indicative of polymer desorption from the SWCNT surface,[67] as the removal of the polymer corona likely altered the dielectric environment around the nanotubes. Thereafter, the fluorescence spectra of the (6,5) and (7,5) SWCNTs were recorded following PFM (Fig. S6). Interestingly, unlike oxygen-defect-incorporated SWCNTs, which typically exhibit an E_{11}^{*} peak alongside the E_{11} peak, no distinct E_{11}^{*} peak was observed. However, in both (6,5) and (7,5) SWCNTs, a notable decrease in the fluorescence of the E_{11} was observed, in concurrence with the reduction in absorption, further supporting the hypothesis of an altered dielectric environment following PFM resulting from partial polymer desorption.[2,68]

The Raman spectrum of PFO-BPy6,6′ (6,5) SWCNTs revealed prominent peaks at 1595 cm^{-1} and 1610 cm^{-1}, attributed to the G band of the SWCNTs[69] and the C=C stretching[70] within the aromatic bipyridine rings of PFO-BPy6,6′ (Fig. 1(A)). Additional peaks spanning 1200–1400 cm^{-1} were also observed, which can be attributed to the polymer. To confirm the peak assignments, we recorded the Raman spectrum of the PFO-BPy6,6′ polymer (Fig. S7), and found all the aforementioned peaks except for the one at 1595 cm^{-1}, suggesting that this peak originates from the SWCNTs. After treatment with NaClO and UV, two significant changes were observed in the PFO-BPy6,6′ (6,5) SWCNTs (Fig. S8). First, the intensity ratio of the 1595 cm^{-1} and 1610 cm^{-1} G band peaks increased significantly, from 1 : 3.03 in untreated SWCNTs to 1 : 1.66 after treatment, suggesting that the PFO-BPy6,6′ corona might be partially removed from the SWCNT surface, as a peak due to PFO-BPy6,6′ was still present. Since Raman spectroscopy was performed on samples deposited on a surface, the observed decrease in the polymer:SWCNT peak ratio directly reflects modifications in the surface-bound polymers. Therefore, the relative decrease in the polymer-related Raman peak, compared to the SWCNT-related Raman peak, suggests that the polymer undergoes partial desorption upon treatment, altering the spectral contributions from the nanotube-polymer interface. Second, a broad peak emerged at 1308 cm^{-1}, the D band, which is typically associated with defect formation in SWCNTs[71] (Fig. S8). However, this peak appeared broad, spanning 1200–1400 cm^{-1}, suggesting the presence of overlapping signals from both polymer-related peaks and the defect-induced peak. In the next step, we sought to eliminate potential interference from polymer-related signals and determine whether the D-band could be clearly resolved, thereby providing unambiguous evidence of defect formation in the (6,5) SWCNTs following PFM. To achieve this, we drop-cast the PFM-treated (6,5) SWCNTs onto a glass slide and washed the films with tetrahydrofuran (THF) to remove any unreacted polymer. Under these conditions, the Raman spectra showed a distinctly resolved D-band at 1303 cm^{-1}, confirming the emergence of defects with improved clarity (Fig. 1(B)). We emphasize that the Raman analysis was employed to confirm the appearance of the defect-related D band and to qualitatively support polymer desorption. The normalized G-band – to polymer peak ratio was included to reinforce this observation within the context of the spectral changes. Nevertheless, the Raman spectral signatures raise the question of why defect incorporation was not reflected in the fluorescence spectra of the SWCNTs *via* an increase in an E_{11}^{*} peak—unlike the typical behavior of defect-incorporated SWCNTs. To address this question, we measured the fluorescence of (6,5) and (7,5) SWCNTs before and after PFM treatment. Our motivation stemmed from the understanding that defects in SWCNTs can undergo thermal detrapping—at room temperature, excitons trapped at defect sites

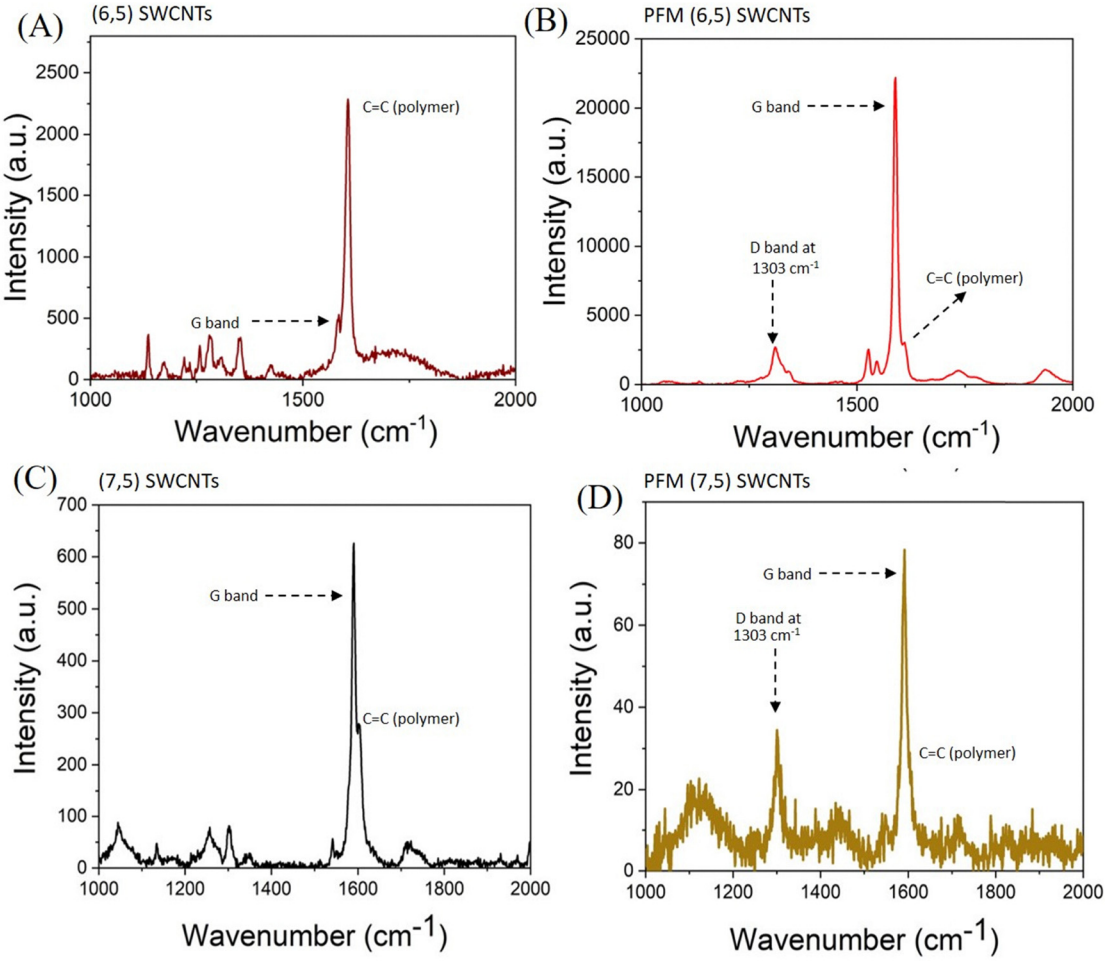

Fig. 1 Raman spectra of PFO-BPy6,6′ (6,5) SWCNTs (A) before and (B) after PFM with NaClO and UV irradiation. Raman spectra of PFO-FH (7,5) SWCNTs (C) before and (D) after PFM with NaClO and UV irradiation.

may acquire sufficient thermal energy to return to the E_{11} state, masking defect-related signatures in the photoluminescence spectrum.[72,73] With this consideration, we conducted fluorescence measurements at 77 K. Interestingly, while the E_{11}-normalized fluorescence spectra of PFM-treated and untreated SWCNTs showed no discernible differences at 298 K (room temperature) (Fig. S9A and B), the 77 K spectra revealed an enhanced E_{11}^{*} peak (with respect to E_{11}) in the PFM samples, confirming the presence of defects (Fig. S9C and D). Additionally, the reduction in E_{11}^{*} intensity following prolonged irradiation, in our case, may have been more pronounced compared to the aqueous medium due to the higher solubility of singlet oxygen in the organic medium.[65] This decrease in E_{11} fluorescence is consistent with prior reports, as such a decrease is commonly observed when defects are introduced into SWCNTs.[58,59] While the emergence of the D-band in Raman spectra and the appearance of E_{11}^{*} emission at low temperature were used to confirm that defects had been introduced, it is important to note that quantitative defect counting could not be reliably extracted from ensemble PL spectra under the present experimental conditions, as defect incorporation is understood to follow inherently stochastic distributions.[74] Further, recent studies have demonstrated that absolute defect quantification is possible by correlating calibrated D/G^{+} ratios and intermediate-frequency Raman modes with known defect densities.[47,71] However, these methods require dedicated calibration standards and defect-controlled reactions. Accurate numerical estimation would have thus required single-nanotube-level measurements, dedicated calibration standards, and defect-controlled reactions, which were beyond the scope of this study. Accordingly, our analysis focuses on the relative and qualitative trends in defect formation rather than on precise quantification.

The process of partial removal of PFO-BPy6,6′ from the surface of (6,5) SWCNTs, followed by the introduction of oxygen defects, is referred to as PFM in this study. To highlight the importance of NaClO and UV in enabling successful PFM in PFO-BPy6,6′ (6,5) SWCNTs, we investigated the independent effects of NaClO and UV. However, when treated with NaClO or UV alone, the Raman characteristics of the PFO-BPy6,6′ (6,5) SWCNTs remained virtually unchanged (Fig. S10A and B). It is worth mentioning that the relatively high ratio of polymer peaks to SWCNT peaks is likely due to the high polymer concentration in the samples, which enhances the polymer Raman contribution relative to the SWCNTs. As control

experiments, the Raman spectra of PFO-BPy6,6′ were recorded both before (Fig. S7) and after treatment with NaClO, UV irradiation, and their combination. Unlike the PFO-BPy6,6′ suspended (6,5) SWCNTs, the polymer alone remained virtually unaffected (Fig. S11A–C). This demonstrated that PFO-BPy6,6′ suspended (6,5) SWCNTs, when subjected to NaClO and UV irradiation, underwent defect incorporation accompanied by partial removal of the PFO-BPy6,6′ corona.

To investigate whether PFO-FH (7,5) SWCNTs undergo partial desorption of their corona similar to PFO-BPy6,6′ (6,5) SWCNTs upon treatment with NaClO and UV irradiation, Raman spectra were recorded. The Raman spectrum of PFO-FH (7,5) SWCNTs displayed two prominent peaks at 1593 cm^{-1} and 1600 cm^{-1}, attributed to the G band of the (7,5) SWCNTs and the C=C stretching within the aromatic part of PFO-FH, respectively (Fig. 1(C)). Additionally, smaller peaks characteristic of polyfluorene-based polymers were observed between 1200 cm^{-1} and 1380 cm^{-1}.[75] To confirm these assignments, the Raman spectrum of PFO-FH alone was acquired (Fig. S12), revealing the characteristic polymer peaks except for the 1593 cm^{-1} peak, which was confirmed to originate from the SWCNTs. Prior to treatment, the intensity ratio of the 1593 cm^{-1} to 1600 cm^{-1} peaks was 2.32 : 1. Following NaClO and UV treatment, the polymer-associated peak at 1600 cm^{-1} became negligible, indicating significant removal of the PFO-FH corona (Fig. 1(D)). Importantly, evidence of defect incorporation was also observed. Following treatment, the polymer-related peak at 1600 cm^{-1} decreased, while a prominent peak emerged at 1303 cm^{-1}, the D band, maintaining an intensity ratio of 1 : 2.2 with the G band of the (7,5) SWCNTs. The appearance of this peak is a clear signature of defect formation. When NaClO and UV were applied independently, the Raman spectra of PFO-FH (7,5) SWCNTs remained practically unchanged (Fig. S13A and B), highlighting the necessity of their combination to achieve PFM. Control experiments further supported this conclusion; Raman spectra of PFO-FH alone, both before and after treatment with NaClO, UV, or their combination (Fig. S14A–C), showed negligible changes. Unlike the PFO-FH-coated (7,5) SWCNTs, the polymer alone remained largely unaffected under all treatment conditions.

After confirming the partial removal of the polymer from the SWCNT surface *via* Raman spectroscopy, we aimed to further validate these findings using dynamic light scattering (DLS), which provides insights into the hydrodynamic diameter of chemical species and any changes upon treatment. To this end, we first measured the hydrodynamic diameter of (6,5) SWCNTs before and after treatment with UV and NaClO. Initially, the hydrodynamic diameter was 128.7 ± 46.7 nm, and decreased to 75.2 ± 5.06 nm following treatment (Fig. 2(A)). This reduction aligns with the partial removal of the polymer stabilizing the SWCNTs. Similarly, for (7,5) SWCNTs, the initial hydrodynamic diameter of 1591 ± 284.6 nm was reduced to 745.3 ± 99.1 nm after treatment (Fig. 2(B)), suggesting a comparable partial removal of the polymer corona.

A key observation is the significant difference in the initial hydrodynamic radius of (6,5) and (7,5) SWCNTs—128.7 ± 46.7 nm *versus* 1591 ± 284.6 nm. While (7,5) SWCNTs have a slightly larger intrinsic diameter (0.83 nm) compared to (6,5) SWCNTs (0.75 nm), this alone cannot account for the nearly tenfold increase in hydrodynamic size. The primary contributing factor is likely the formation of a multilayer coating on the SWCNTs by PFO,[29] and, by extension, PFO-FH due to its structural similarity. This multilayer coating likely accounts for the larger hydrodynamic diameter observed for (7,5) SWCNTs compared to (6,5) SWCNTs. According to our experience, PFO-BPy6,6′ necessitates much lower polymer:SWCNT ratios to selectively extract (6,5) SWCNTs, whereas heteroatom-free PFO-derivatives demand substantially higher polymer:SWCNT ratios to isolate chirality-pure (7,5) SWCNTs.[29,76] This is the first time the dramatic dissimilarities in behavior of the two most commonly used conjugated polymers (PFO-BPy6,6′ and a structurally-similar derivative of PFO) for selective SWCNT solubilization have been observed in solution.

Next, we aimed to assess the surface coverage of SWCNTs before and after PFM treatment, with the hypothesis that polymer desorption during PFM might expose more surface area. To probe this, we employed molecular probe analysis (MPA) using RB, a fluorophore known to adsorb onto SWCNT surfaces.[12,77] RB exhibits an emission peak at 560 nm when excited at 460 nm. We measured its fluorescence before and after adding it to separate solutions of (6,5), (7,5), PFM (6,5), and PFM (7,5) SWCNTs. Upon addition of (6,5) and (7,5) SWCNTs, only a slight decrease in RB fluorescence was observed, indicating minimal adsorption and thus limited exposed surface area (Fig. 2(C) and (D)). In contrast, the addition of PFM (6,5) and (7,5) SWCNTs led to a marked decrease in RB fluorescence, implying significantly greater adsorption and increased surface accessibility (Fig. 2(E) and (F)). To rule out any direct quenching effect of NaClO and UV treatment on RB, we performed a control experiment where RB was treated with NaClO and UV independently. The fluorescence remained largely unchanged (Fig. S15), confirming that the observed quenching in the presence of PFM SWCNTs resulted from RB adsorption onto newly exposed nanotube surfaces. This provided further evidence of polymer desorption following PFM, leading to enhanced surface availability. In the next step, we investigated the impact of PFM on the structural characteristics of SWCNTs. Our hypothesis was that if the polymers were indeed being removed from the SWCNT surface, a reduction in the SWCNT diameter would be observed. To test this, we acquired TEM images of (6,5) polymer-coated SWCNTs, which revealed well-dispersed nanotubes with an average diameter of 7.03 ± 0.9 nm. After PFM, the SWCNTs remained well-dispersed, but their average diameter decreased to 4.02 ± 0.6 nm (Fig. S16A and D). Similarly, for (7,5) polymer-coated SWCNTs, the TEM images showed well-separated nanotubes with an initial average diameter of 9.25 ± 0.7 nm, which reduced to 6.23 ± 0.1 nm following PFM (Fig. S17A–D). These observations indicate partial removal of the polymer corona, leading to a measurable decrease in SWCNTs diameter.

Furthermore, since a decrease in both absorption and fluorescence emission was observed for (6,5) and (7,5) SWCNTs following PFM, it was crucial to confirm experimentally that

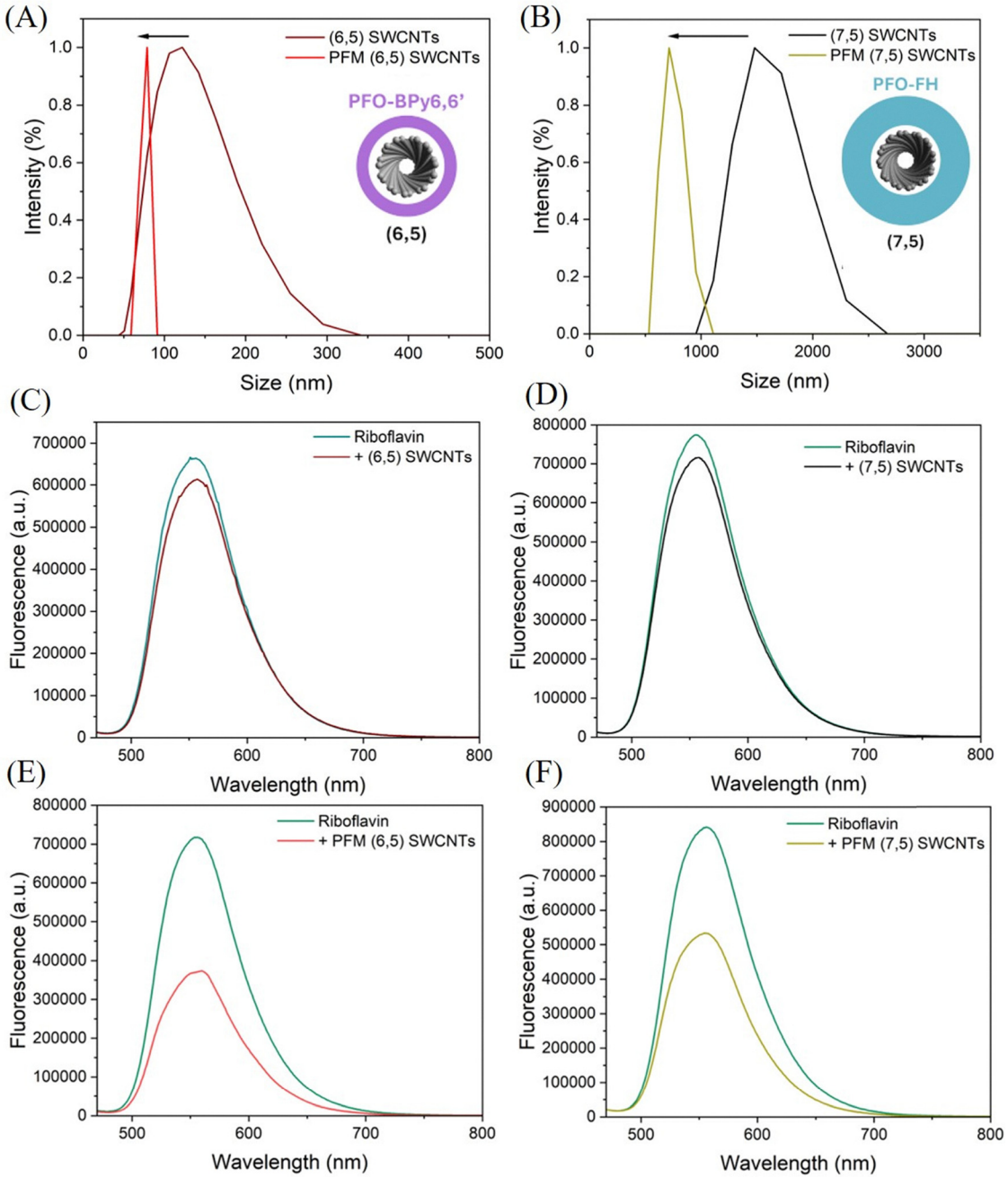

Fig. 2 DLS measurement of (A) (6,5) SWCNTs (dark brown) and PFM (6,5) SWCNTs (red) and (B) (7,5) SWCNTs and PFM (7,5) SWCNTs. Fluorescence spectra of RB before and after the addition of (C) (6,5) SWCNTs, (D) (7,5) SWCNTs, (E) PFM (6,5) SWCNTs, and (F) PFM (7,5) SWCNTs.

their colloidal stability was not compromised. The fluorescence of the PFM-treated SWCNTs remained stable for nearly 24 h, indicating that polymer removal caused a one-time decrease in fluorescence, after which no further decrease was observed (Fig. S18A and B). Since only a small fraction of the polymer was detached from the SWCNT surface, the dispersion stability was not compromised, while the possibility of chemical modification was enabled. The well-dispersed nature of the (6,5) and (7,5) SWCNTs, as evident from TEM images, clearly demonstrated that their colloidal stability remained intact. Thus, the observed decrease in absorption and fluorescence emission could be attributed largely to polymer removal, ruling out the possibility of aggregation following PFM.

The above experimental findings pointed toward partial polymer removal from the SWCNT surface. To further characterize the polymer released from the SWCNTs, we employed UV-vis-NIR spectroscopy. We began by measuring the absorption spectra of (6,5) and (7,5) SWCNTs before and after PFM treatment. In the subsequent step, these samples, including PFM-treated and untreated variants, were filtered using a 100 kDa molecular weight cutoff filter, and the absorption spectra of the resulting filtrates were recorded. Interestingly, the filtrates

from untreated (6,5) and (7,5) SWCNTs showed no discernible polymer-related absorption features. In contrast, the filtrates from PFM-treated (6,5) and (7,5) SWCNTs exhibited a distinct absorption peak at 380 nm, characteristic of the polymer. This result clearly indicates that polymer desorption occurred following PFM and that the detached polymer was successfully eluted in the filtrate upon filtration (Fig. S19). To assess the extent of polymer desorption from the (6,5) and (7,5) SWCNTs following PFM, we first recorded the UV-vis-NIR spectra of the as-prepared dispersions, which showed the characteristic polymer absorption peaks at 360 nm for PFO-BPy6,6′ and 380 nm for PFO-FH. Filtration through an Amicon membrane yielded filtrates without these peaks, indicating that the polymer remained bound to the SWCNTs under these conditions. In contrast, after PFM treatment, filtration of the sample produced filtrates that clearly displayed the corresponding polymer peaks, confirming polymer release. By comparing the polymer absorbance associated with the SWCNTs before PFM with the absorbance observed in the filtrate after PFM, we estimated that 12.02% and 4.62% of the polymer desorbed from the (6,5) and (7,5) SWCNTs, respectively. Building on the above findings, we present a schematic illustration depicting the partial desorption of the polymer from the SWCNT surface and the defect incorporation (Scheme 1).

A key limitation of organic corona-stabilized SWCNTs lies in the tight wrapping of the corona around the nanotubes,[32] which effectively shields them from interacting with exogenously added molecules. Our PFM strategy addresses this challenge through the partial removal of the corona while maintaining colloidal stability, thereby unlocking the surface of the SWCNTs for enhanced molecular interactions. By overcoming this fundamental barrier, our approach not only resolves a critical issue in the field but also paves the way for the exploration of the responsiveness of polymer-stabilized SWCNTs to external analytes, broadening their applicability in sensing and functional nanotechnology. Moreover, monochiral SWCNTs were selected to provide uniform diameters and well-defined optical signatures, thereby enabling more precise interpretation of analyte-SWCNTs interactions. This controlled structural and photophysical uniformity allowed the fluorescence responses to be attributed more reliably to the introduced sensitivity rather than to heterogeneity within the nanotube population.

After developing a PFM-based strategy to partly remove the SWCNTs' corona with the goal of imparting reactivity, we proceeded to assess its effectiveness. Among the chemical functionalities retained on the PFM-SWCNTs and SWCNT surfaces, the π-conjugated rings of the residual polymers stand out. These π rings are well-suited for engaging in π–π stacking interactions with exogenously introduced molecules that possess similar π-conjugated structures.[78–82] PAHs provide an ideal test set for this interaction, as their progressively increasing number of fused aromatic rings offers a systematic way to probe how surface accessibility and π–π stacking strength scale with analyte size. With this concept in mind, the PFM-treated (6,5) and (7,5) SWCNTs were exposed to poly-π-conjugated molecules—specifically, naphthalene (Naph), phenanthrene (Phen), pyrene, and fluorene.

While only a minimal fluorescence response was observed for non-PFM (6,5) SWCNTs (Fig. 3(A)–(D)), a pronounced fluorescence response was induced in PFM-treated (6,5) SWCNTs upon exposure to Naph, Phen, pyrene, and fluorene (Fig. 3(E)–(H)). This striking behavior was likely driven by the partial removal of the polymer corona, which facilitated direct interactions with external molecules, leading to a concentration-dependent fluorescence decrease. These findings highlight the transformative potential of PFM in overcoming the inherent reactivity barriers of organic polymer-stabilized SWCNTs, enabling them to interact effectively with exogenously added molecules through complementary functionalities, such as π–π stacking, as discussed in the current study.

Additional experiments were conducted with PFO-FH (7,5) SWCNTs to further emphasize the efficacy of PFM in rendering them responsive to functional molecules. As seen with the non-PFM (6,5) SWCNTs, no significant change in fluorescence was observed for non-PFM PFO-FH (7,5) SWCNTs when exposed to Naph, Phen, pyrene, and fluorene (Fig. 4(A)–(D)). However, when PFM PFO-FH (7,5) SWCNTs were treated with these analytes, fluorescence decrease was clearly observed (Fig. 4(E)–(H)), with the extent of the intensity response increased with the concentrations of the PAHs.

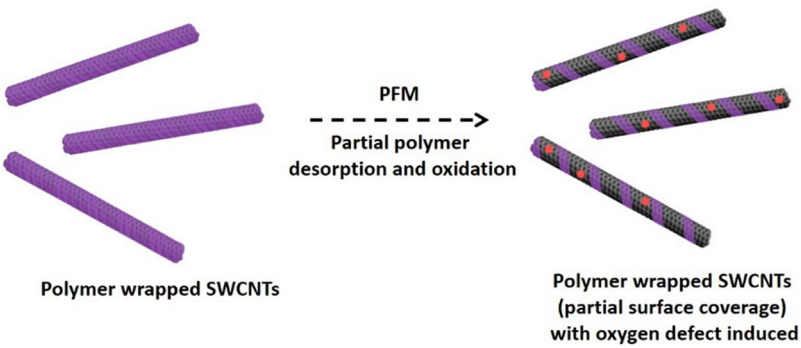

Scheme 1 A schematic illustration depicting the PFM process: the addition of NaClO, followed by UV exposure, results in partial desorption of polymers from the SWCNTs' surface and incorporation of oxygen defects.

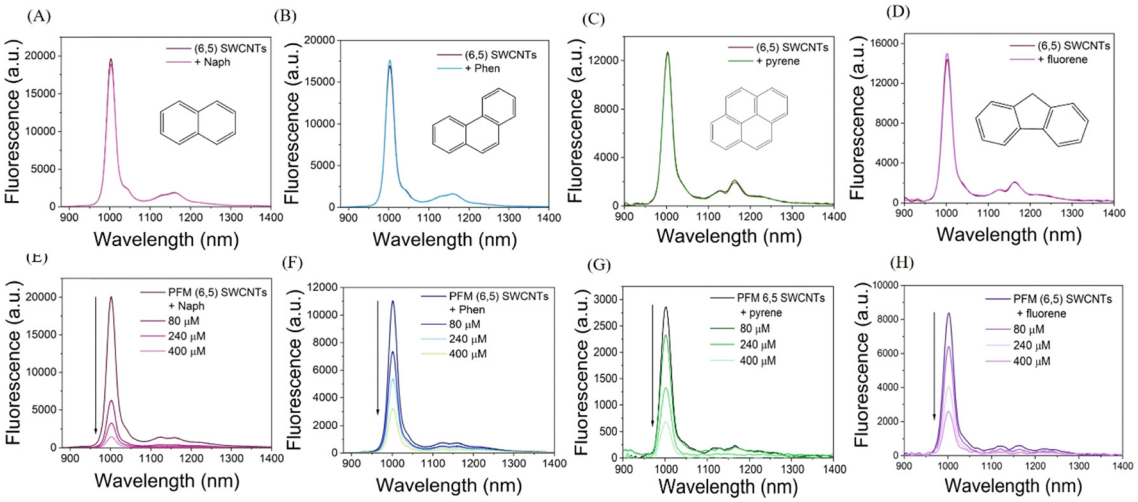

Fig. 3 Fluorescence spectra of (6,5) SWCNTs before and after the addition of 400 μM of (A) Naph, (B) Phen, (C) pyrene, and (D) fluorene. Fluorescence spectra of PFM (6,5) SWCNTs before and after the addition of varying concentrations of (E) Naph, (F) Phen, (G) pyrene, and (H) fluorene.

These collective findings not only underscore the transformative potential of PFM in enhancing the reactivity and sensitivity of polymer-stabilized SWCNTs but also highlight its broad applicability for detecting a wide range of exogenously added molecules through tailored molecular interactions.

To definitively attribute the fluorescence response of PFM PFO-BPy6,6′ (6,5) SWCNTs and PFM PFO-FH (7,5) SWCNTs to polycyclic aromatic hydrocarbons (PAHs) like Naph and Phen, pyrene, and fluorene, we investigated the impact of adding non-PAH molecules, such as monoaromatic compounds with varying side groups. Additionally, aliphatic chain-containing molecules were incubated with PFM PFO-BPy6,6′ (6,5) SWCNTs and PFM PFO-FH (7,5) SWCNTs to evaluate their influence on the fluorescence response. Specifically, we tested 1,3,5-triethylbenzene, 1,3,5-trimethoxybenzene, anisole, and bromohexane (Fig. S20). Interestingly, none of these molecules induced a fluorescence intensity decrease comparable to that caused by PAHs like Naph and Phen. These findings highlight the critical role of polyaromatic systems in eliciting fluorescence responses from PFM SWCNTs, primarily due to π–π stacking interactions.

Building on these findings, we set to demonstrate that while the monomeric form of a molecule containing a single benzene ring would not induce a fluorescence response in SWCNTs, its polymeric counterpart containing multiple benzene rings would exhibit a response similar to that observed with PAHs. To test this hypothesis, styrene and polystyrene were selected as model compounds. Interestingly, when PFM-treated (6,5) and (7,5) SWCNTs were incubated with styrene, no significant change in fluorescence was observed (Fig. S21A and B). However, upon interaction with polystyrene, a noticeable decrease in fluorescence was detected in both SWCNT types (Fig. S21C and D). These results clearly demonstrate that the fluorescence response of PFM-SWCNTs to PAHs is driven by π–π stacking interactions, requiring at least two aromatic rings in the

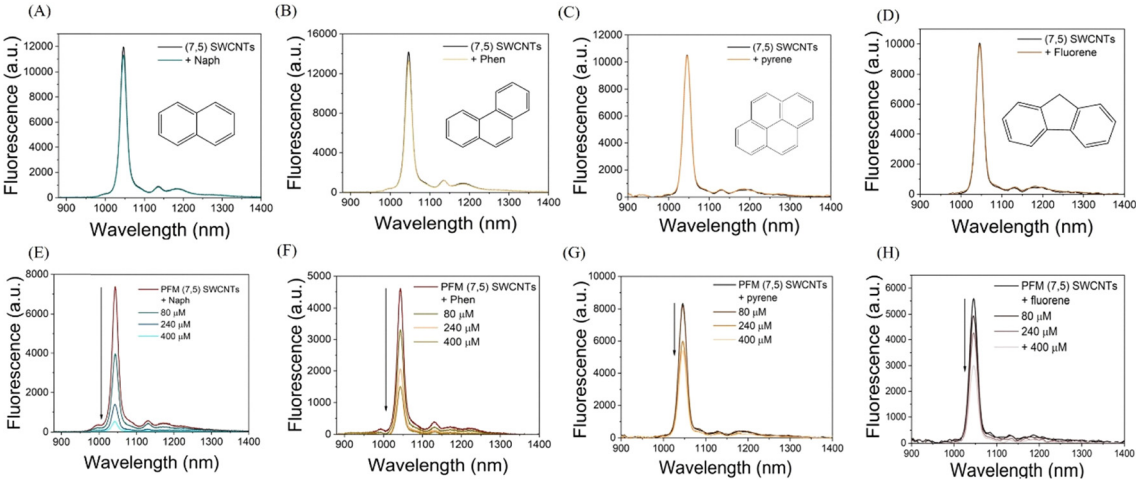

Fig. 4 Fluorescence spectra of (7,5) SWCNTs before and after the addition of 400 μM of (A) Naph, (B) Phen, (C) pyrene, and (D) fluorene. Fluorescence spectra of PFM (7,5) SWCNTs before and after the addition of varying concentrations of (E) Naph, (F) Phen, (G) pyrene, and (H) fluorene.

externally introduced molecules to elicit a measurable fluorescence response. Moreover, the effect of a polycyclic aliphatic compound such as decalin on the fluorescence of PFM (6,5) and (7,5) SWCNTs was also examined. Unlike PAHs, decalin, a saturated naphthalene, did not elicit a fluorescence decrease in the PFM SWCNTs (Fig. S22). These results indicated that the presence of π-groups was required to induce a fluorescence decrease in the PFM SWCNTs.

Next, it has been proposed that fluorophores involved in π–π stacking interactions exhibit a concomitant decrease in quantum yield (QY).[83] Therefore, the QYs of PFM-(6,5) and PFM-(7,5) SWCNTs were evaluated following their interaction with PAHs to further support the proposed π–π stacking mechanism of the PFM-SWCNTs fluorescence decrease. To this end, relative QY estimations were carried out using well-established reference standards, namely, rhodamine B (excitation at 560 nm) for PFM-(6,5) SWCNTs and Cy5 (excitation at 650 nm) for PFM-(7,5) SWCNTs. The QYs of PFM-(6,5) and PFM-(7,5) SWCNTs were calculated to be 0.79% and 0.52%, respectively. However, upon the addition of 400 μM of Naph, Phen, fluorene, and pyrene, the QYs of PFM-(6,5) SWCNTs decreased to 0.39%, 0.24%, 0.13%, and 0.22%, respectively (Table S1), and the QYs of PFM-(7,5) SWCNTs decreased to 0.37%, 0.26%, 0.43%, and 0.39%, respectively (Table S2). This decrease in quantum yield of the PFM-SWCNTs upon PAH addition strongly supports the presence of π–π stacking interactions, aligning with the observed decrease in their fluorescence intensity. Although general PL quenching is inherently nonspecific, our PFM strategy transformed this optical response into a controllable and mechanistically meaningful tool for tuning SWCNT surface accessibility, ultimately enabling size-selective reactivity toward PAHs. The fluorescence decrease observed for the PFM-treated SWCNTs upon interaction with PAHs through non-covalent π–π stacking is further supported by previous reports demonstrating that SWCNTs with exposed surfaces readily interact with PAHs.[84–86] Further, the absence of any discernible fluorescence response in the polymer-wrapped SWCNTs prior to PFM strongly suggests that their surfaces were not sufficiently exposed to enable such interactions, thereby highlighting the role of controlled polymer removal *via* PFM in facilitating PAH accessibility.[84–86] These findings provide additional validation for the proposed non-covalent interaction mechanism between the PFM-SWCNTs and the PAHs. In addition to non-covalent interactions, the PAHs may also facilitate charge transfer between the SWCNTs and the PAH molecules.[87] Khoerunnisa *et al.* reported that naphthalene or naphthalene-derivatives, which are PAHs, when adsorbed on SWCNTs, change their electronic characteristics.[88] Moreover, Campo and co-workers showed that the optical properties of SWCNTs are affected by the general presence of hydrocarbons.[89] The possibility of making van der Waals interactions of PAHs with SWCNTs enhances this phenomenon and facilitates stable adsorption.

Subsequently, we aimed to discern whether the surface coverage of SWCNTs could be tuned through PFM by varying the concentration of NaClO used during treatment. Since corona displacement plays a critical role in determining the accessibility of the SWCNT surface, establishing a controllable method to modulate this parameter would provide a direct handle on their interactive behavior. To probe such variations in surface coverage, RB was employed as a fluorescence reporter, as its emission is readily quenched when adsorbed onto accessible SWCNT surfaces.[77,90] By systematically altering the NaClO concentration and monitoring the extent of RB quenching, we sought to establish a correlation between PFM conditions and corona density, thereby enabling a rational strategy to fine-tune SWCNT responsiveness toward external analytes. We selected naphthalene, fluorene, and pyrene, representing ring sizes of two, three, and four, respectively, from the set of naphthalene, phenanthrene, fluorene, and pyrene. For (6,5) SWCNTs, RB fluorescence revealed a clear dependence on NaClO treatment (Fig. 5(A)). At low NaClO concentrations (0.01%), quenching was minimal, consistent with dense polymer coverage restricting RB access to the nanotube surface. Increasing the NaClO concentration progressively enhanced quenching, with an increased concentration of NaClO to 0.02% and with the strongest effect observed at 0.055%,

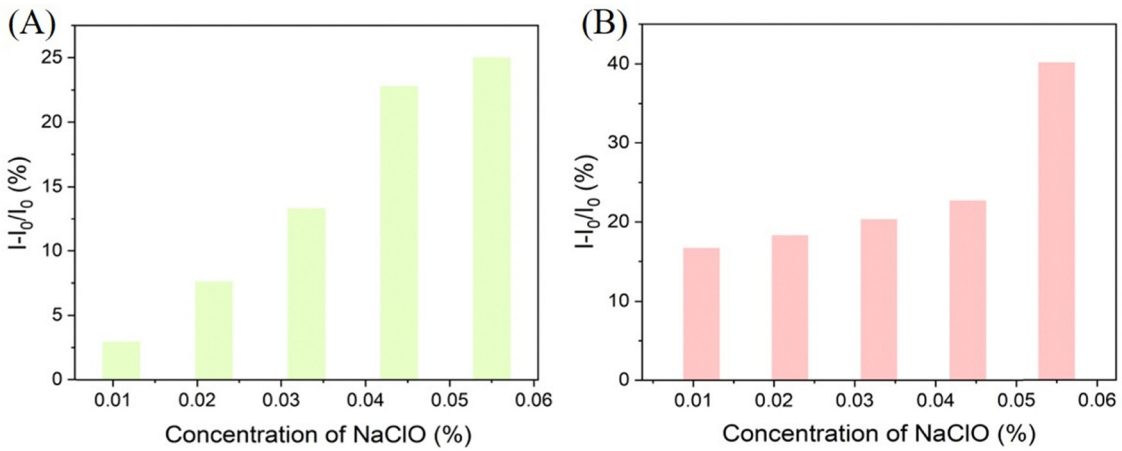

Fig. 5 Extent of RB fluorescence decrease following the addition of PFM-treated (A) (6,5) and (B) (7,5) SWCNTs across different NaClO concentrations.

indicative of reduced surface coverage and greater accessibility of the SWCNT surface. Intermediate treatments produced graded responses, confirming that corona density on (6,5) SWCNTs can be systematically tuned through PFM.

For (7,5) SWCNTs, a similar trend was observed (Fig. 5(B)). Minimal quenching occurred at low NaClO concentrations, reflecting high surface coverage, whereas higher concentrations led to progressively stronger RB quenching, with maximum quenching at 0.055% NaClO. This demonstrates that corona displacement in (7,5) SWCNTs can also be controlled by adjusting NaClO levels, paralleling the behavior seen in (6,5) SWCNTs. Together, these results establish PFM as a generalizable approach to modulate surface coverage across different SWCNT chiralities, thereby providing a controllable handle to tune their responsiveness toward external analytes.

Having established that surface coverage can be tuned through PFM, we next examined how these variations influence the fluorescence response of SWCNTs toward PAHs. For (6,5) SWCNTs, treatment with a low NaClO concentration (0.01%) did not elicit any response to Naph, fluorene, or pyrene, consistent with dense surface coverage restricting analyte access (Fig. 6(A)–(C)). At an intermediate NaClO concentration (0.02%), a selective fluorescence decrease was observed only in the presence of Naph, 2-rings containing PAH, with negligible

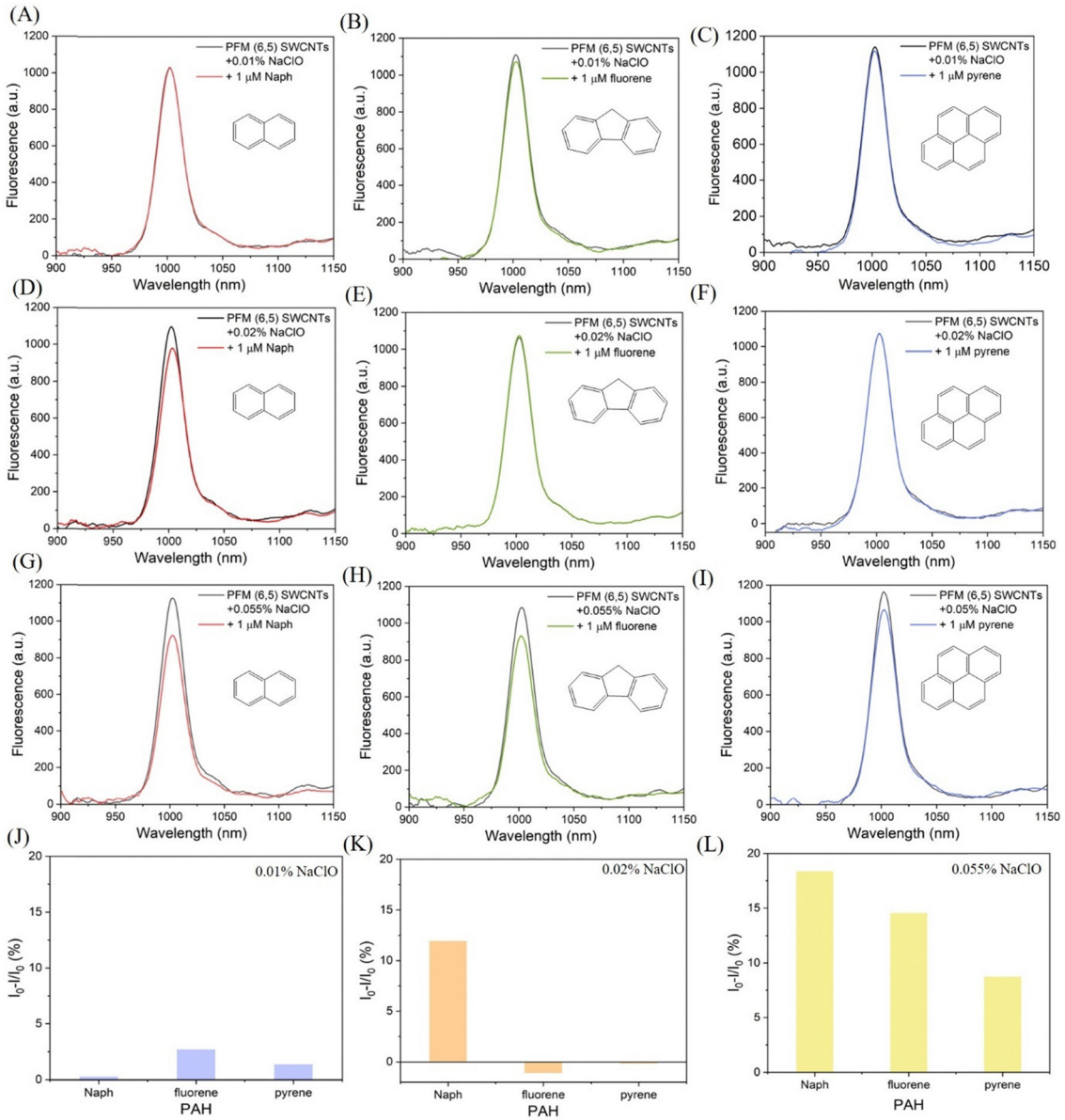

Fig. 6 Fluorescence spectra of (6,5) SWCNTs treated with (A)–(C) 0.01%, (D)–(F) 0.02%, and (G)–(I) 0.055% NaClO, acquired before and after the addition of Naph, fluorene, and pyrene, respectively. Panels (J)–(L) show the corresponding bar graphs illustrating the extent of fluorescence change for each analyte under the different NaClO treatment conditions, highlighting the effect of surface coverage on size-selective fluorescence response.

response to fluorene (3-rings containing PAH) or pyrene (4-rings containing PAH) (Fig. 6(D)–(F)). At higher NaClO concentration (0.055%), corresponding to reduced surface coverage, the fluorescence response broadened to include all three PAHs, namely, Naph, fluorene, and pyrene (Fig. 6(G)–(I)). The fluorescence responses for each condition are summarized in a bar graph (Fig. 6(J)–(L)), where the relative decrease in fluorescence intensities is plotted against the different PAHs, clearly illustrating the transition from no response (0.01%) to selective response (0.02%) and finally to broad-spectrum response (0.05%).

A parallel trend was observed for (7,5) SWCNTs, where 0.01% treatment produced no response (Fig. 7(A)), 0.02% enabled selective interaction with Naph (Fig. 7(B)), and 0.055% resulted in fluorescence response to all three PAHs (Fig. 7(C)). The corresponding bar graph for (7,5) SWCNTs (Fig. 7(D)) shows this progression, highlighting the absence of response at 0.01% NaClO, the selective response to Naph at 0.02% NaClO, and the broadened response to Naph, fluorene, and pyrene at 0.05% NaClO. These results establish a direct correlation between corona density and analyte size selectivity, demonstrating that PFM provides not only enhanced reactivity but also a mechanism to tune fluorescence response modes from non-responsive, to selective, and finally to broad-spectrum detection.

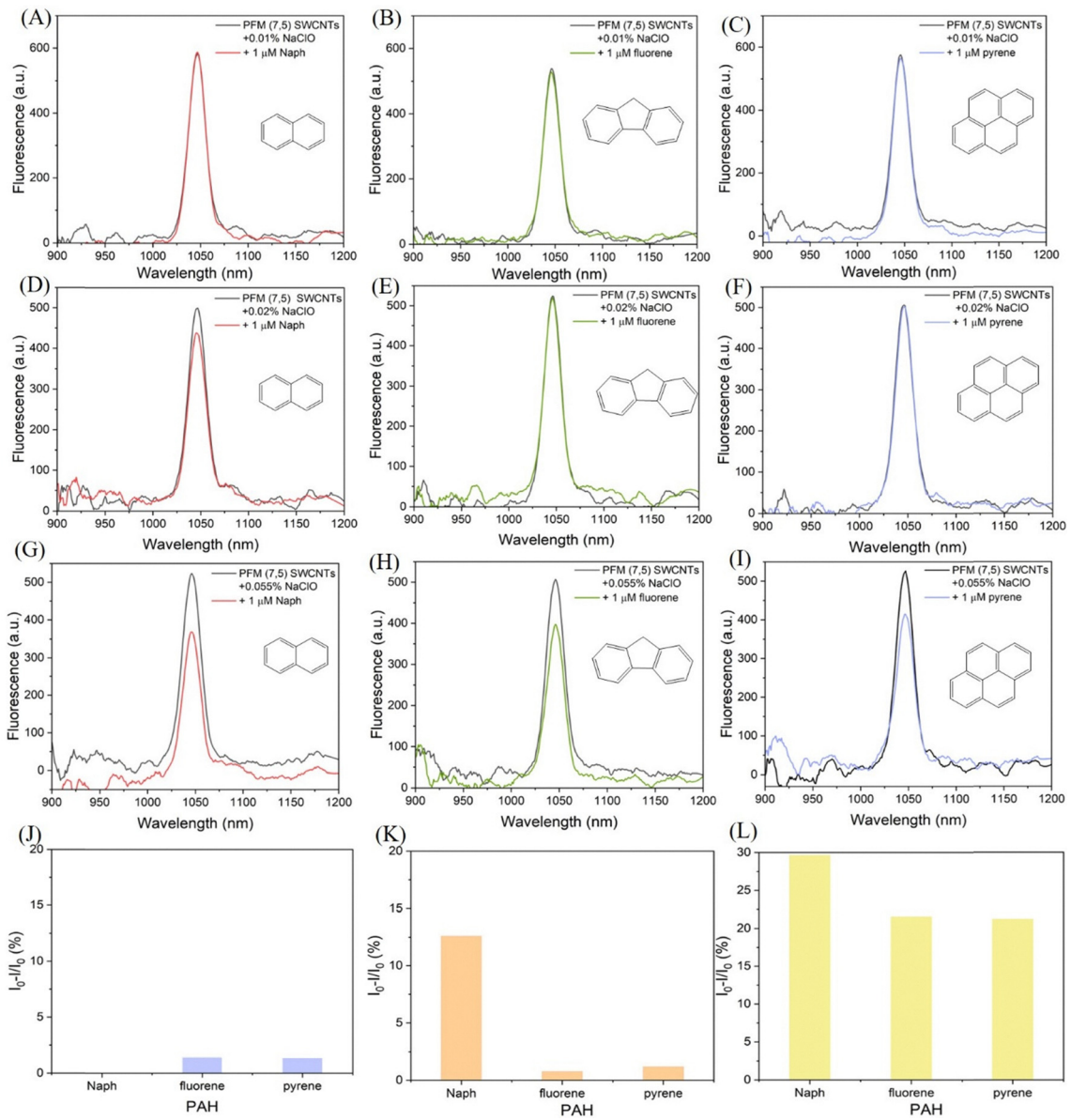

Fig. 7 Fluorescence spectra of (7,5) SWCNTs treated with (A)–(C) 0.01%, (D)–(F) 0.02%, and (G)–(I) 0.055% NaClO, acquired before and after the addition of Naph, fluorene, and pyrene, respectively. Panels (J)–(L) show the corresponding bar graphs illustrating the extent of fluorescence decrease for each analyte under the different NaClO treatment conditions, highlighting the effect of surface coverage on size-selective fluorescence response.

4. Conclusions

We successfully demonstrated the application of the post-functionalization modification (PFM) as an effective strategy to enhance the responsiveness of single-walled carbon nanotubes (SWCNTs) dispersed in organic media. By exposing chirality-pure (6,5) and (7,5) SWCNTs to sodium hypochlorite (NaClO) and UV irradiation, we achieved partial polymer corona displacement and oxygen defects incorporation, as confirmed through Raman spectroscopy, dynamic light scattering (DLS), and transmission electron microscopy (TEM). The PFM SWNCTs featured significant fluorescence response to the polyaromatic hydrocarbons (PAHs) like naphthalene, phenanthrene, pyrene, and fluorene, in stark contrast to the unmodified polymer-suspended SWCNTs, which showed minimal to no fluorescence response to the PAH analytes tested. Furthermore, the role of polyaromaticity in fluorescence modulation was evident, as PFM (6,5) and (7,5) SWCNTs displayed a strong response to polystyrene, while exhibiting negligible fluorescence changes upon interaction with styrene monomers. Crucially, we demonstrated that the degree of corona displacement, and thereby the accessibility of the SWCNT surface, could be systematically tuned through the concentration of NaClO during PFM. This tunability directly translated into size-selective adsorption of PAHs: intermediate surface coverage favored selective recognition of smaller molecules such as naphthalene, while reduced coverage enabled a broader response encompassing larger PAHs like fluorene and pyrene. Furthermore, Quantum Yield (QY) estimations before and after PAH addition further supported the role of these interactions in fluorescence quenching. Further, QY estimations of PFM-(6,5) and PFM-(7,5) SWCNTs before and after PAH addition revealed a marked decrease in QY, thereby providing additional support for the proposed π–π stacking interaction as the underlying mechanism for fluorescence decrease of the SWCNTs. Together, these findings highlight PFM as a versatile and controllable approach to impart reactivity to otherwise inert SWCNTs. While the literature has previously established that polymer coverage on SWCNTs depends on polymer concentration, our objective here is to address the fundamental question of how SWCNTs wrapped with a given polymer concentration could be post-functionally modified through our PFM approach to enable size-selective reactivity toward PAHs. Beyond enabling molecular recognition in organic media, the demonstrated tunability and size-selectivity open exciting avenues for the design of SWCNT-based sensing platforms where selective *versus* broad-spectrum detection can be dialed in by controlled surface modification. Moreover, in this work, we establish a robust experimental framework that clarifies how controlled polymer desorption and defect introduction modulate the photophysical response of SWCNTs. These trends provide the essential mechanistic basis for designing calibrated readouts, thereby laying a solid foundation for future quantitative sensing schemes. Collectively, our results offer both the conceptual groundwork and the experimental leeway needed to advance this system toward practical, quantitative detection applications.

Conflicts of interest

The authors declare no conflict of interest.

Data availability

Data supporting this article have been incorporated in the supplementary information (SI). Supplementary information is available. See DOI: https://doi.org/10.1039/d5mh02318a.

Acknowledgements

GB acknowledges the support of the Zuckerman STEM Leadership Program, the Naomi Prawer Kadar Foundation, the Moonshot Research Seed Funding in Bio-Nanotechnology, the ERC NanoNonEq 101039127, the Israel Science Foundation (grant no. 196/22), the Ministry of Science, Technology, and Space, Israel (grant no. 1001818370 and 0008452), the Zimin Institute for Engineering Solutions Advancing Better Lives, the Nicholas and Elizabeth Slezak Super Center for Cardiac Research and Biomedical Engineering at Tel Aviv University, and the Marian Gertner Institute for Medical Nanosystems at Tel Aviv University. SB thanks the Centre for Nanotechnology, Indian Institute of Technology Guwahati, for extending the fluorescence measurement facility acquired through funds received from the Ministry of Electronics and Information Technology *via* the INUP-I2I program (5(1)/2021-NANO) and the SWASTHA COE (5(1)/2022-NANO). This project has been co-funded by the Department of Atomic Energy (project no: VS8/SIN/414), Government of India. SB also thanks Mr Santanu Dolai, Dr Archismita Hajra, Mr Shamim Hossain Shah, and Ujjala Dey for their help with AFM and TEM measurements. DJ and DJ acknowledge the National Science Centre, Poland (under the SONATA program, Grant agreement UMO-2020/39/D/ST5/00285) for co-funding this research.

References

1 R. Jin, C. Zeng, M. Zhou and Y. Chen, Atomically Precise Colloidal Metal Nanoclusters and Nanoparticles: Fundamentals and Opportunities, *Chem. Rev.*, 2016, **116**(18), 10346–10413, DOI: 10.1021/acs.chemrev.5b00703.

2 J. Ackermann, J. T. Metternich, S. Herbertz and S. Kruss, Biosensing with Fluorescent Carbon Nanotubes, *Angew. Chem., Int. Ed.*, 2022, **61**(18), e202112372, DOI: 10.1002/anie.202112372.

3 L. Qiu and F. Ding, Understanding Single-Walled Carbon Nanotube Growth for Chirality Controllable Synthesis, *Acc. Mater. Res.*, 2021, **2**(9), 828–841, DOI: 10.1021/accountsmr.1c00111.

4 S. Basu, A. Hendler-Neumark and G. Bisker, Dynamic Tracking of Biological Processes Using Near-Infrared Fluorescent Single-Walled Carbon Nanotubes, *ACS Appl. Mater. Interfaces*, 2024, **16**(41), 54960–54975, DOI: 10.1021/acsami.4c10955.

5 S. Basu, A. Hendler-Neumark and G. Bisker, Monitoring Enzyme Activity Using Near-Infrared Fluorescent Single-Walled Carbon

Nanotubes, *ACS Sens.*, 2024, **9**(5), 2237–2253, DOI: 10.1021/acssensors.4c00377.

6 R. Nißler, F. A. Mann, H. Preiß, G. Selvaggio, N. Herrmann and S. Kruss, Chirality enriched carbon nanotubes with tunable wrapping *via* corona phase exchange purification (CPEP), *Nanoscale*, 2019, **11**(23), 11159–11166, DOI: 10.1039/C9NR03258D.

7 Z. Cohen and R. M. Williams, Single-Walled Carbon Nanotubes as Optical Transducers for Nanobiosensors *In Vivo*, *ACS Nano*, 2024, **18**(52), 35164–35181, DOI: 10.1021/acsnano.4c13076.

8 A. T. Krasley, E. Li, J. M. Galeana, C. Bulumulla, A. G. Beyene and G. S. Demirer, Carbon Nanomaterial Fluorescent Probes and Their Biological Applications, *Chem. Rev.*, 2024, **124**(6), 3085–3185, DOI: 10.1021/acs.chemrev.3c00581.

9 A. Setaro, M. Adeli, M. Glaeske, D. Przyrembel, T. Bisswanger, G. Gordeev, F. Maschietto, A. Faghani, B. Paulus and M. Weinelt, *et al.*, Preserving π-conjugation in covalently functionalized carbon nanotubes for optoelectronic applications, *Nat. Commun.*, 2017, **8**(1), 14281, DOI: 10.1038/ncomms14281.

10 X. Liu, J. Chen, H. Wang, B. Lambert and A. A. Boghossian, Cation Pretreatment Enables the Saline Stability of a Near-Infrared Sensor for Dopamine, *ACS Bio & Med Chem Au*, 2025, **5**(1), 166–174, DOI: 10.1021/acsbiomedchemau.4c00094.

11 Y. Lee, W. Kim, Y. Cho, M. Yoon, S. Lee, J. Lee, S. Oh, Y. Song, B. J. Lee and Y. Kim, *et al.*, Rational Design of 3D Polymer Corona Interfaces of Single-Walled Carbon Nanotubes for Receptor-Free Virus Recognition, *ACS Nano*, 2024, **18**(20), 13214–13225, DOI: 10.1021/acsnano.4c02130.

12 S. Lee, G. Ryu, S. Shin, W. Kim, M. Yoon, Y. Kim, S. Park, Y. Kim and S.-Y. Cho, Clinically-Driven Rapidly Developed Nanoparticle Corona for Label-Free Cerebrospinal Fluid Leakage Detection, *ACS Nano*, 2025, **19**(1), 950–962, DOI: 10.1021/acsnano.4c12364.

13 S. Basu, A. Hendler-Neumark and G. Bisker, Rationally Designed Functionalization of Single-Walled Carbon Nanotubes for Real-Time Monitoring of Cholinesterase Activity and Inhibition in Plasma, *Small*, 2024, 2309481, DOI: 10.1002/smll.202309481.

14 F. Yang, M. Wang, D. Zhang, J. Yang, M. Zheng and Y. Li, Chirality Pure Carbon Nanotubes: Growth, Sorting, and Characterization, *Chem. Rev.*, 2020, **120**(5), 2693–2758, DOI: 10.1021/acs.chemrev.9b00835.

15 R. Nißler, L. Kurth, H. Li, A. Spreinat, I. Kuhlemann, B. S. Flavel and S. Kruss, Sensing with Chirality-Pure Near-Infrared Fluorescent Carbon Nanotubes, *Anal. Chem.*, 2021, **93**(16), 6446–6455, DOI: 10.1021/acs.analchem.1c00168.

16 D. Just, A. Dzienia, K. Z. Milowska, A. Mielańczyk and D. Janas, High-yield and chirality-selective isolation of single-walled carbon nanotubes using conjugated polymers and small molecular chaperones, *Mater. Horiz.*, 2024, **11**(3), 758–767, DOI: 10.1039/D3MH01687K.

17 B. Podlesny, B. Olszewska, Z. Yaari, P. V. Jena, G. Ghahramani, R. Feiner, D. A. Heller and D. Janas, En route to single-step, two-phase purification of carbon nanotubes facilitated by high-throughput spectroscopy, *Sci. Rep.*, 2021, **11**(1), 10618, DOI: 10.1038/s41598-021-89839-4.

18 J. A. Fagan, Aqueous two-polymer phase extraction of single-wall carbon nanotubes using surfactants, *Nanoscale Adv.*, 2019, **1**(9), 3307–3324, DOI: 10.1039/C9NA00280D.

19 M. Zheng, A. Jagota, E. D. Semke, B. A. Diner, R. S. McLean, S. R. Lustig, R. E. Richardson and N. G. Tassi, DNA-assisted dispersion and separation of carbon nanotubes, *Nat. Mater.*, 2003, **2**(5), 338–342, DOI: 10.1038/nmat877.

20 A. Khalid, W. Yi, S. Yoo, S. Abbas, J. Si, X. Hou and J. Hou, Single-chirality of single-walled carbon nanotubes (SWCNTs) through chromatography and its potential biological applications, *New J. Chem.*, 2023, **47**(3), 992–1022, DOI: 10.1039/D2NJ04056E.

21 Y. Li, L. Li, H. Jiang, L. Qian, M. He, D. Zhou, K. Jiang, H. Liu, X. Qin and Y. Gao, *et al.*, An efficient approach toward production of near-zigzag single-chirality carbon nanotubes, *Sci. Adv.*, 2024, **10**(14), eadn6519, DOI: 10.1126/sciadv.adn6519.

22 X. Zhou, P. Wang, Y. Li, Y. Han, J. Chen, K. Tang, L. Shi, Y. Zhang, R. Zhang and Z. Lin, Accurate DNA Sequence Prediction for Sorting Target-Chirality Carbon Nanotubes and Manipulating Their Functionalities, *ACS Nano*, 2025, **19**(2), 2665–2676, DOI: 10.1021/acsnano.4c14603.

23 C. M. Sims, M. Zheng and J. A. Fagan, Single-wall carbon nanotube separations via aqueous two-phase extraction: new prospects enabled by high-throughput methods, *Chem. Commun.*, 2025, **61**(10), 2026–2039, DOI: 10.1039/D4CC06096B.

24 J. A. Fagan, E. H. Hároz, R. Ihly, H. Gui, J. L. Blackburn, J. R. Simpson, S. Lam, A. R. Hight Walker, S. K. Doorn and M. Zheng, Isolation of >1 nm Diameter Single-Wall Carbon Nanotube Species Using Aqueous Two-Phase Extraction, *ACS Nano*, 2015, **9**(5), 5377–5390, DOI: 10.1021/acsnano.5b01123.

25 N. K. Subbaiyan, S. Cambré, A. N. G. Parra-Vasquez, E. H. Hároz, S. K. Doorn and J. G. Duque, Role of Surfactants and Salt in Aqueous Two-Phase Separation of Carbon Nanotubes toward Simple Chirality Isolation, *ACS Nano*, 2014, **8**(2), 1619–1628, DOI: 10.1021/nn405934y.

26 B. Podlesny, K. R. Hinkle, K. Hayashi, Y. Niidome, T. Shiraki and D. Janas, Highly-Selective Harvesting of (6,4) SWCNTs Using the Aqueous Two-Phase Extraction Method and Non-ionic Surfactants, *Adv. Sci.*, 2023, **10**(14), 2207218, DOI: 10.1002/advs.202207218.

27 L. Li, D. Yang, X. Li, W. Wang, X. Wei, W. Zhou and H. Liu, High-Efficiency Separation of Near-Zigzag Single-Chirality Carbon Nanotubes by Gel Chromatography, *Phys. Status Solidi B*, 2025, 2400322, DOI: 10.1002/pssb.202400322.

28 Y. Yomogida, T. Tanaka, M. Zhang, M. Yudasaka, X. Wei and H. Kataura, Industrial-scale separation of high-purity single-chirality single-wall carbon nanotubes for biological imaging, *Nat. Commun.*, 2016, **7**(1), 12056, DOI: 10.1038/ncomms12056.

29 A. Dzienia, D. Just, T. Wasiak, K. Z. Milowska, A. Mielańczyk, N. Labedzki, S. Kruss and D. Janas, Size Matters in Conjugated Polymer Chirality-Selective SWCNT Extraction, *Adv. Sci.*, 2024, **11**(29), 2402176, DOI: 10.1002/advs.202402176.

30 A. Dzienia, D. Just, P. Taborowska, A. Mielanczyk, K. Z. Milowska, S. Yorozuya, S. Naka, T. Shiraki and D. Janas, Mixed-Solvent Engineering as a Way around the Trade-Off between Yield and Purity of (7,3) Single-Walled Carbon Nanotubes Obtained Using Conjugated Polymer Extraction, *Small*, 2023, **19**(46), 2304211, DOI: 10.1002/smll.202304211.
31 D. Fong and A. Adronov, Recent developments in the selective dispersion of single-walled carbon nanotubes using conjugated polymers, *Chem. Sci.*, 2017, **8**(11), 7292–7305, DOI: 10.1039/C7SC02942J.
32 J. M. Salazar-Rios, W. Talsma, V. Derenskyi, W. Gomulya, T. Keller, M. Fritsch, S. Kowalski, E. Preis, M. Wang and S. Allard, *et al.*, Understanding the Selection Mechanism of the Polymer Wrapping Technique toward Semiconducting Carbon Nanotubes, *Small Methods*, 2018, **2**(4), 1700335, DOI: 10.1002/smtd.201700335.
33 S. Basu, C. Gayen, S. Dolai and A. Paul, Tailoring the luminescence of atomic clusters via ligand exchange reaction mediated post synthetic modification, *Phys. Chem. Chem. Phys.*, 2020, **22**(7), 3959–3964, DOI: 10.1039/C9CP06063D.
34 S. Basu, M. P. Bakulić, H. Fakhouri, I. Russier-Antoine, C. Moulin, P.-F. Brevet, V. Bonačić-Koutecký and R. Antoine, Rationale Strategy to Tune the Optical Properties of Gold Catenane Nanoclusters by Doping with Silver Atoms, *J. Phys. Chem. C*, 2020, **124**(35), 19368–19374, DOI: 10.1021/acs.jpcc.0c05402.
35 S. Pramanik, S. Bhandari, S. Roy and A. Chattopadhyay, Synchronous Tricolor Emission-Based White Light from Quantum Dot Complex, *J. Phys. Chem. Lett.*, 2015, **6**(7), 1270–1274, DOI: 10.1021/acs.jpclett.5b00295.
36 P. V. Ravi, V. Subramaniyam and M. Pichumani, Influence of in-situ and post-modification syntheses on the characteristic properties of tyrosine functionalized graphene quantum dots, *Diamond Relat. Mater.*, 2022, **128**, 109229, DOI: 10.1016/j.diamond.2022.109229.
37 A. Pal, M. P. Sk and A. Chattopadhyay, Recent advances in crystalline carbon dots for superior application potential, *Mater. Adv.*, 2020, **1**(4), 525–553, DOI: 10.1039/D0MA00108B.
38 M. Kalaj and S. M. Cohen, Postsynthetic Modification: An Enabling Technology for the Advancement of Metal–Organic Frameworks, *ACS Cent. Sci.*, 2020, **6**(7), 1046–1057, DOI: 10.1021/acscentsci.0c00690.
39 W. He, D. Lv, Y. Guan and S. Yu, Post-synthesis modification of metal–organic frameworks: synthesis, characteristics, and applications, *J. Mater. Chem. A*, 2023, **11**(45), 24519–24550, DOI: 10.1039/D3TA05158G.
40 S. Bhandari, S. Pramanik, R. Khandelia and A. Chattopadhyay, Gold Nanocluster and Quantum Dot Complex in Protein for Biofriendly White-Light-Emitting Material, *ACS Appl. Mater. Interfaces*, 2016, **8**(3), 1600–1605, DOI: 10.1021/acsami.6b00039.
41 S. Pramanik, S. Roy, A. Mondal and S. Bhandari, A two-target responsive reversible ratiometric pH nanoprobe: a white light emitting quantum dot complex, *Chem. Commun.*, 2019, **55**(30), 4331–4334, DOI: 10.1039/C9CC01088B.
42 S. Basu and N. Amdursky, The Role of Surface Groups in Dictating the Chiral-Solvent-Induced Assembly of Carbon Dots into Structures Exhibiting Circularly Polarized Luminescence, *Small*, 2023, 2205880, DOI: 10.1002/smll.202205880.
43 S. O. Hunter, A. Nikolich, M. R. Bryant, D. Skelton and C. Richardson, Dual metal organic framework post-synthetic modification; two birds with one stone, *Chem. Commun.*, 2024, **60**, 14822–14825, DOI: 10.1039/D4CC04987J.
44 C. Ma, J. M. Mohr, G. Lauer, J. T. Metternich, K. Neutsch, T. Ziebarth, A. Reiner and S. Kruss, Ratiometric Imaging of Catecholamine Neurotransmitters with Nanosensors, *Nano Lett.*, 2024, **24**(7), 2400–2407, DOI: 10.1021/acs.nanolett.3c05082.
45 S. Settele, C. A. Schrage, S. Jung, E. Michel, H. Li, B. S. Flavel, A. S. K. Hashmi, S. Kruss and J. Zaumseil, Ratiometric fluorescent sensing of pyrophosphate with sp^3-functionalized single-walled carbon nanotubes, *Nat. Commun.*, 2024, **15**(1), 706, DOI: 10.1038/s41467-024-45052-1.
46 F. A. Mann, N. Herrmann, F. Opazo and S. Kruss, Quantum Defects as a Toolbox for the Covalent Functionalization of Carbon Nanotubes with Peptides and Proteins, *Angew. Chem., Int. Ed.*, 2020, **59**(40), 17732–17738, DOI: 10.1002/anie.202003825.
47 F. L. Sebastian, F. Becker, Y. Yomogida, Y. Hosokawa, S. Settele, S. Lindenthal, K. Yanagi and J. Zaumseil, Unified Quantification of Quantum Defects in Small-Diameter Single-Walled Carbon Nanotubes by Raman Spectroscopy, *ACS Nano*, 2023, **17**(21), 21771–21781, DOI: 10.1021/acsnano.3c07668.
48 J. Zaumseil, Luminescent Defects in Single-Walled Carbon Nanotubes for Applications, *Adv. Opt. Mater.*, 2022, **10**(2), 2101576, DOI: 10.1002/adom.202101576.
49 M. Kim, J. J. McCann, J. Fortner, E. Randall, C. Chen, Y. Chen, Z. Yaari, Y. Wang, R. L. Koder and D. A. Heller, Quantum Defect Sensitization via Phase-Changing Supercharged Antibody Fragments, *J. Am. Chem. Soc.*, 2024, **146**(18), 12454–12462, DOI: 10.1021/jacs.4c00149.
50 B. J. Heppe, N. Dzombic, J. M. Keil, X.-L. Sun and G. Ao, Solvent Isotope Effects on the Creation of Fluorescent Quantum Defects in Carbon Nanotubes by Aryl Diazonium Chemistry, *J. Am. Chem. Soc.*, 2023, **145**(47), 25621–25631, DOI: 10.1021/jacs.3c07341.
51 C.-W. Lin, S. M. Bachilo, Y. Zheng, U. Tsedev, S. Huang, R. B. Weisman and A. M. Belcher, Creating fluorescent quantum defects in carbon nanotubes using hypochlorite and light, *Nat. Commun.*, 2019, **10**(1), 2874, DOI: 10.1038/s41467-019-10917-3.
52 S. Ghosh, S. M. Bachilo, R. A. Simonette, K. M. Beckingham and R. B. Weisman, Oxygen Doping Modifies Near-Infrared Band Gaps in Fluorescent Single-Walled Carbon Nanotubes, *Science*, 2010, **330**(6011), 1656–1659, DOI: 10.1126/science.1196382.
53 A. K. Mandal, X. Wu, J. S. Ferreira, M. Kim, L. R. Powell, H. Kwon, L. Groc, Y. Wang and L. Cognet, Fluorescent sp3 Defect-Tailored Carbon Nanotubes Enable NIR-II Single Particle Imaging in Live Brain Slices at Ultra-Low Excitation Doses, *Sci. Rep.*, 2020, **10**(1), 5286, DOI: 10.1038/s41598-020-62201-w.

54 A. H. Brozena, M. Kim, L. R. Powell and Y. Wang, Controlling the optical properties of carbon nanotubes with organic colour-centre quantum defects, *Nat. Rev. Chem.*, 2019, **3**(6), 375–392, DOI: 10.1038/s41570-019-0103-5.

55 Y. Niidome, H. Matsumoto, R. Hamano, K. Kato, T. Fujigaya and T. Shiraki, Polymer Wrapping State Changes at Defect Sites of Locally Functionalized Single-Walled Carbon Nanotubes, *J. Phys. Chem. C*, 2024, **128**(12), 5146–5155, DOI: 10.1021/acs.jpcc.3c07692.

56 V. B. Espinoza, S. M. Bachilo, Y. Zheng, H. Htoon and R. B. Weisman, Complexity in the Photofunctionalization of Single-Wall Carbon Nanotubes with Hypochlorite, *ACS Nano*, 2025, **19**(2), 2497–2506, DOI: 10.1021/acsnano.4c13605.

57 A. A. Alizadehmojarad, S. M. Bachilo and R. B. Weisman, Guanine Functionalization of Single-Wall Carbon Nanotubes: A Quantum Chemical Study, *ACS Nano*, 2025, **19**(22), 21038–21045, DOI: 10.1021/acsnano.5c04839.

58 S. Basu, A. Hendler-Neumark and G. Bisker, Role of Oxygen Defects in Eliciting a Divergent Fluorescence Response of Single-Walled Carbon Nanotubes to Dopamine and Serotonin, *ACS Nano*, 2024, **18**(50), 34134–34146, DOI: 10.1021/acsnano.4c10360.

59 S. Basu, A. Hendler-Neumark and G. Bisker, Ratiometric Normalization of Near-Infrared Fluorescence in Defect-Engineered Single-Walled Carbon Nanotubes for Cholesterol Detection, *J. Phys. Chem. Lett.*, 2024, **15**(42), 10425–10434, DOI: 10.1021/acs.jpclett.4c02022.

60 A. M. Shetty, G. M. H. Wilkins, J. Nanda and M. J. Solomon, Multiangle Depolarized Dynamic Light Scattering of Short Functionalized Single-Walled Carbon Nanotubes, *J. Phys. Chem. C*, 2009, **113**(17), 7129–7133, DOI: 10.1021/jp900731q.

61 S. Badaire, P. Poulin, M. Maugey and C. Zakri, In Situ Measurements of Nanotube Dimensions in Suspensions by Depolarized Dynamic Light Scattering, *Langmuir*, 2004, **20**(24), 10367–10370, DOI: 10.1021/la049096r.

62 A. Krasulina, Y. Myasnikova, V. Saik, M. Predtechensky and S. N. Smirnov, Improved Characterization of Aqueous Single-Walled Carbon Nanotube Dispersions Using Dynamic Light Scattering and Analytical Centrifuge Methods, *ACS Omega*, 2023, **8**(42), 39233–39241, DOI: 10.1021/acsomega.3c04639.

63 A. Graf, Y. Zakharko, S. P. Schießl, C. Backes, M. Pfohl, B. S. Flavel and J. Zaumseil, Large scale, selective dispersion of long single-walled carbon nanotubes with high photoluminescence quantum yield by shear force mixing, *Carbon*, 2016, **105**, 593–599, DOI: 10.1016/j.carbon.2016.05.002.

64 I. Sudakov, E. Goovaerts, W. Wenseleers, J. L. Blackburn, J. G. Duque and S. Cambré, Chirality Dependence of Triplet Excitons in (6,5) and (7,5) Single-Wall Carbon Nanotubes Revealed by Optically Detected Magnetic Resonance, *ACS Nano*, 2023, **17**(3), 2190–2204, DOI: 10.1021/acsnano.2c08392.

65 M. Bregnhøj, F. Thorning and P. R. Ogilby, Singlet Oxygen Photophysics: From Liquid Solvents to Mammalian Cells, *Chem. Rev.*, 2024, **124**(17), 9949–10051, DOI: 10.1021/acs.chemrev.4c00105.

66 M. M. Mburu, A.-N. Au-Duong, W.-T. Li, W.-Y. Yu, Y.-W. Lan, W.-H. Chiang and Y.-C. Chiu, Highly Stable Single-Walled Carbon Nanotube Sorting by Low Molecular Weight Conjugated Polymer with Hydrogen-Bonded Polyisoprene, *Adv. Electron. Mater.*, 2022, **8**(12), 2200698, DOI: 10.1002/aelm.202200698.

67 A. Dutta, S. Das, A. Paul and A. Chattopadhyay, Kinetics of reaction of gold nanoparticles following partial removal of stabilizers, *J. Nanopart. Res.*, 2015, **17**(6), 260, DOI: 10.1007/s11051-015-3021-6.

68 D. A. Heller, G. W. Pratt, J. Zhang, N. Nair, A. J. Hansborough, A. A. Boghossian, N. F. Reuel, P. W. Barone and M. S. Strano, Peptide secondary structure modulates single-walled carbon nanotube fluorescence as a chaperone sensor for nitroaromatics, *Proc. Natl. Acad. Sci. U. S. A.*, 2011, **108**(21), 8544–8549, DOI: 10.1073/pnas.1005512108.

69 Y. Park, K. P. S. S. Hembram, R. Yoo, B. Jang, W. Lee, S.-G. Lee, J.-G. Kim, Y.-I. Kim, D. J. Moon and J.-K. Lee, *et al.*, Reinterpretation of Single-Wall Carbon Nanotubes by Raman Spectroscopy, *J. Phys. Chem. C*, 2019, **123**(22), 14003–14009, DOI: 10.1021/acs.jpcc.9b02174.

70 N. Félidj, S. L. Truong, J. Aubard, G. Lévi, J. R. Krenn, A. Hohenau, A. Leitner and F. R. Aussenegg, Gold particle interaction in regular arrays probed by surface enhanced Raman scattering, *J. Chem. Phys.*, 2004, **120**(15), 7141–7146, DOI: 10.1063/1.1676152(acccessed 12/10/2024).

71 F. L. Sebastian, N. F. Zorn, S. Settele, S. Lindenthal, F. J. Berger, C. Bendel, H. Li, B. S. Flavel and J. Zaumseil, Absolute Quantification of sp3 Defects in Semiconducting Single-Wall Carbon Nanotubes by Raman Spectroscopy, *J. Phys. Chem. Lett.*, 2022, **13**(16), 3542–3548, DOI: 10.1021/acs.jpclett.2c00758.

72 F. L. Sebastian, S. Settele, H. Li, B. S. Flavel and J. Zaumseil, How to recognize clustering of luminescent defects in single-wall carbon nanotubes, *Nanoscale Horiz.*, 2024, **9**(12), 2286–2294, DOI: 10.1039/D4NH00383G.

73 M. Kim, L. Adamska, N. F. Hartmann, H. Kwon, J. Liu, K. A. Velizhanin, Y. Piao, L. R. Powell, B. Meany and S. K. Doorn, *et al.*, Fluorescent Carbon Nanotube Defects Manifest Substantial Vibrational Reorganization, *J. Phys. Chem. C*, 2016, **120**(20), 11268–11276, DOI: 10.1021/acs.jpcc.6b02538.

74 C. Ma, C. A. Schrage, J. Gretz, A. Akhtar, L. Sistemich, L. Schnitzler, H. Li, K. Tschulik, B. S. Flavel and S. Kruss, Stochastic Formation of Quantum Defects in Carbon Nanotubes, *ACS Nano*, 2023, **17**(16), 15989–15998, DOI: 10.1021/acsnano.3c04314.

75 A. Perevedentsev, N. Chander, J.-S. Kim and D. D. C. Bradley, Spectroscopic properties of poly(9,9-dioctylfluorene) thin films possessing varied fractions of β-phase chain segments: enhanced photoluminescence efficiency *via* conformation structuring, *J. Polym. Sci., Part B:Polym. Phys.*, 2016, **54**(19), 1995–2006, DOI: 10.1002/polb.24106.

76 D. Just, T. Wasiak, A. Dzienia, K. Z. Milowska, A. Mielańczyk and D. Janas, Explicating conjugated polymer extraction used for the differentiation of single-walled carbon nanotubes, *Nanoscale Horiz.*, 2024, **9**(12), 2349–2359, DOI: 10.1039/D4NH00427B.

77 M. Park, D. P. Salem, D. Parviz, X. Gong, K. S. Silmore, T. T. S. Lew, D. T. Khong, M. C.-Y. Ang, S.-Y. Kwak and

M. B. Chan-Park, *et al.*, Measuring the Accessible Surface Area within the Nanoparticle Corona Using Molecular Probe Adsorption, *Nano Lett.*, 2019, **19**(11), 7712–7724, DOI: 10.1021/acs.nanolett.9b02647.

78 E. M. Pérez and N. Martín, π–π interactions in carbon nanostructures, *Chem. Soc. Rev.*, 2015, **44**(18), 6425–6433, DOI: 10.1039/C5CS00578G.

79 C. Roquelet, J.-S. Lauret, V. Alain-Rizzo, C. Voisin, R. Fleurier, M. Delarue, D. Garrot, A. Loiseau, P. Roussignol and J. A. Delaire, *et al.*, Π-Stacking Functionalization of Carbon Nanotubes through Micelle Swelling, *ChemPhysChem*, 2010, **11**(8), 1667–1672, DOI: 10.1002/cphc.201000067.

80 V. Wulf and G. Bisker, Integrating Single-Walled Carbon Nanotubes into Supramolecular Assemblies: From Basic Interactions to Emerging Applications, *ACS Nano*, 2024, **18**(43), 29380–29393, DOI: 10.1021/acsnano.4c06843.

81 T. Chen, M. Li and J. Liu, π–π Stacking Interaction: A Nondestructive and Facile Means in Material Engineering for Bioapplications, *Cryst. Growth Des.*, 2018, **18**(5), 2765–2783, DOI: 10.1021/acs.cgd.7b01503.

82 L. Francis; N. Shoichi; J. C. Francis; D. H. Joshua; Y. Dabin; L. Alison; C. Linda; M. Aishwarya and P. L. Markita, Covalent Attachment of Horseradish Peroxidase to Single-Walled Carbon Nanotubes for Hydrogen Peroxide Detection. *bioRxiv*, preprint, 2023, 2023.2012.2014.571773, DOI: 10.1101/2023.12.14.571773.

83 H. Bhatia, S. Dey and D. Ray, Effect of π···π Interactions of Donor Rings on Persistent Room-Temperature Phosphorescence in D4–A Conjugates and Data Security Application, *ACS Omega*, 2021, **6**(5), 3858–3865, DOI: 10.1021/acsomega.0c05666.

84 J. Yoo, H. Ozawa, T. Fujigaya and N. Nakashima, Evaluation of affinity of molecules for carbon nanotubes, *Nanoscale*, 2011, **3**(6), 2517–2522, DOI: 10.1039/C1NR10079C.

85 S. Gotovac, H. Honda, Y. Hattori, K. Takahashi, H. Kanoh and K. Kaneko, Effect of Nanoscale Curvature of Single-Walled Carbon Nanotubes on Adsorption of Polycyclic Aromatic Hydrocarbons, *Nano Lett.*, 2007, **7**(3), 583–587, DOI: 10.1021/nl0622597.

86 T.-A. Chao, C.-P. Chuu, S.-L. Liew, I.-F. Hu, S.-K. Su, S. Li, S.-C. Lin, V. D.-H. Hou, H.-S. P. Wong and I. Radu, *et al.*, Small Molecule Additives to Suppress Bundling in Dimensional-Limited Self-Alignment Method for High-Density Aligned Carbon Nanotube Array, *Adv. Mater. Interfaces*, 2024, **11**(6), 2300684, DOI: 10.1002/admi.202300684.

87 Z. Kuang, F. J. Berger, J. L. P. Lustres, N. Wollscheid, H. Li, J. Lüttgens, M. B. Leinen, B. S. Flavel, J. Zaumseil and T. Buckup, Charge Transfer from Photoexcited Semiconducting Single-Walled Carbon Nanotubes to Wide-Bandgap Wrapping Polymer, *J. Phys. Chem. C*, 2021, **125**(15), 8125–8136, DOI: 10.1021/acs.jpcc.0c10171.

88 F. Khoerunnisa, A. Morelos-Gomez, H. Tanaka, T. Fujimori, D. Minami, R. Kukobat, T. Hayashi, S. Y. Hong, Y. C. Choi and M. Miyahara, *et al.*, Metal–semiconductor transition like behavior of naphthalene-doped single wall carbon nanotube bundles, *Faraday Discuss.*, 2014, **173**, 145–156, DOI: 10.1039/C4FD00119B.

89 J. Campo, S. Cambré, B. Botka, J. Obrzut, W. Wenseleers and J. A. Fagan, Optical Property Tuning of Single-Wall Carbon Nanotubes by Endohedral Encapsulation of a Wide Variety of Dielectric Molecules, *ACS Nano*, 2021, **15**(2), 2301–2317, DOI: 10.1021/acsnano.0c08352.

90 G. Sánchez-Velázquez, D. T. Khong, M. Park, X. Jin, Z. Yuan, X. Gong, M. C.-Y. Ang and M. S. Strano, Using Molecular Probe Adsorption to Characterize the Nanoparticle Corona Phase and Molecular Recognition, *Langmuir*, 2025, **41**(27), 17602–17614, DOI: 10.1021/acs.langmuir.5c01222.